LETTERS
PUBLISHED ONLINE: 31 OCTOBER 2010 | DOI: 10.1038/NPHYS1810
nature physics

Optimal control of vortex-core polarity by resonant microwave pulses

Benjamin Pigeau[1], Grégoire de Loubens[1]*, Olivier Klein[1], Andreas Riegler[2], Florian Lochner[2], Georg Schmidt[2]† and Laurens W. Molenkamp[2]

In a vortex-state magnetic nanodisc[1–3], the static magnetization curls in the plane, except in the core region, where it points out of plane[4,5], either up or down, leading to two possible stable states of opposite core polarity *p*. Dynamical reversal of *p* by large-amplitude motion of the vortex core[6–9] has recently been demonstrated experimentally[10–14], raising the prospect of practical applications, in particular in magnetic-storage devices[15]. Here we demonstrate coherent control of *p* by single- and double-microwave-pulse sequences, taking advantage of the resonant vortex dynamics in a perpendicular-bias magnetic field[16]. Experimental optimization of the microwave-pulse duration required for switching *p* also yields information about the characteristic decay time of the vortex core in the large-oscillation regime. This time is found to be less than half the length seen in the small-oscillation regime, suggesting a nonlinear behaviour of magnetic dissipation.

Magnetic vortices are topological solitons with rich dynamical properties. The lowest-energy excitation of the vortex ground state is the so-called gyrotropic mode[3], corresponding to the gyration of the vortex core around its equilibrium position with a frequency in the sub-gigahertz range[17,18]. It is now established experimentally[14] that the excitation of this gyrotropic motion leads to a dynamical distortion of the vortex-core profile, as predicted by micromagnetic simulations and theoretical analysis[8]. This distortion increases with the linear velocity of the vortex core and opposes the core polarity, until the critical velocity $V_c \simeq 1.66\gamma\sqrt{A_{ex}}$ (γ is the gyromagnetic ratio of the magnetic material and A_{ex} its exchange constant) is reached and the vortex-core polarity is reversed[9].

In zero magnetic field, dynamical control of the polarity is difficult owing to the degeneracy of the gyrotropic frequencies associated with opposite polarities $p = \pm 1$, which can lead to multiple core switching[7,11]. Still, selective core-polarity reversal is possible using a circularly polarized microwave magnetic field because the sense of the core rotation is linked by a right-hand rule to its polarity[12]. Control of polarity switching can also be achieved by precise timing of non-resonant magnetic-field pulses[13,19], in a similar fashion as domain-wall propagation in magnetic nanowires[20].

Resonant amplification[21] of the vortex gyrotropic motion enables us to reverse the core polarity with minimum excitation power[12,14,15], as it enables us to concentrate the energy in a narrow frequency band. In this scheme, the damping ratio is an important parameter because it controls the minimum amplitude of the resonant excitation required to switch the core[9]. Here, it is shown that the damping ratio close to the reversal threshold is significantly larger than that measured in the small-oscillation regime. We associate this with the nonlinear nature of the reversal process[6,8].

Investigation of vortex-core reversal using time-resolved imaging techniques based on X-ray magnetic circular dichroism is very powerful, as it enables direct determination of the vortex-core trajectory[14]. However, it requires averaging of many events and the interpretation can become more complicated owing to multiple reversal processes. In order to investigate the coupling between resonant microwave pulses and vortex dynamics near the core-reversal threshold, we use a magnetic resonance force microscope (MRFM) in combination with a bias magnetic field applied perpendicularly to the disc plane, that induces two distinct resonant gyrotropic frequencies associated with opposite core polarities[16,22]. This frequency splitting is used for a simple, single-shot reading[15] of the polarity state using an MRFM, before and after microwave pulses have been applied to the vortex-state nanodisc.

The MRFM detection set-up[23], illustrated in Fig. 1a, is described in the Methods section. It enables us to probe the magnetization dynamics in individual nanostructures[24], and in particular to spectroscopically determine the resonance frequency of the gyrotropic mode in a vortex-state nanodisc[16]. The studied nanodisc with thickness 44 nm and diameter 1 μm is made of NiMnSb alloy (see the magnetic-force-microscope image in Fig. 1b), an ultralow-damping epitaxial material[25] (the typical Gilbert constant α_{LLG} is between 0.002 and 0.003). A gold antenna patterned on top enables us to apply pulses of linearly polarized microwave magnetic field h in the plane of the disc.

In our experiments, we choose the bias perpendicular field $\mu_0 H = 65$ mT to unambiguously discriminate the two different gyrotropic frequencies, or polarity states: resonant frequencies $f_- = 217$ MHz and $f_+ = 254$ MHz respectively correspond to $p = -1$ (core antiparallel to H, see Fig. 1d) and $p = +1$ (core parallel to H, see Fig. 1c). The microwave power employed to read the polarity state with an MRFM is weak enough ($P = -19$ dBm) that p is not reversed during the reading sequence[15]. We also emphasize that the bias perpendicular field $\mu_0 H = 65$ mT is almost five times smaller than the static field required to switch the core polarity[16,26], so no significant asymmetry between the two possible reversal processes ($p = -1$ to $p = +1$ and vice versa) is induced, as will be clear from the data presented below.

First, we explore in Fig. 2a the efficiency of single microwave pulses to switch the vortex core, depending on their duration, frequency and power. Π_- pulses are defined as single pulses that reverse the polarity from $p = -1$ to $p = +1$ and Π_+ pulses from $p = +1$ to $p = -1$ (see Fig. 2b). The experimental data are acquired as follows: for Π_- (Π_+) pulses, the $p = -1$ ($p = +1$) state is first reset using an initialization pulse whose result is known to be fully deterministic[15]. Then, a single microwave pulse of given duration

[1]Service de Physique de l'État Condensé (CNRS URA 2464), CEA Saclay, 91191 Gif-sur-Yvette, France, [2]Physikalisches Institut (EP3), Universität Würzburg, 97074 Würzburg, Germany. †Present address: Institut für Physik, Martin-Luther-Universität, Halle Wittenberg, 06099 Halle, Germany.
*e-mail: gregoire.deloubens@cea.fr.

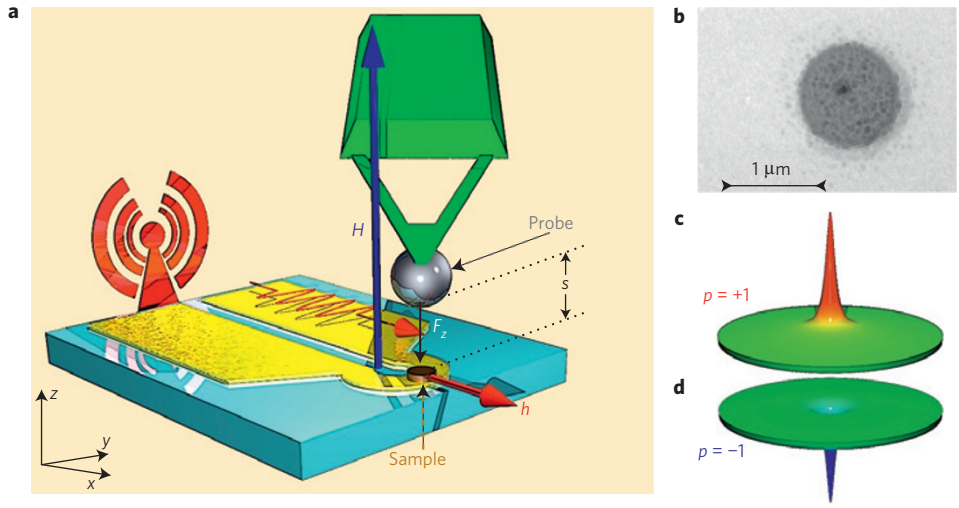

Figure 1 | Experimental set-up and sample. a, An MRFM (see Methods) is used to probe the vortex-core dynamics of an individual vortex-state NiMnSb disc (diameter 1 μm, thickness 44 nm). A soft cantilever, with a spherical magnetic probe attached at its end and placed at a distance $s = 1.5$ μm from the sample, detects mechanically the vortex-core dynamics. The bias magnetic field H is applied perpendicularly to the disc plane whereas microwave pulses of linearly polarized field h are applied in the plane. **b**–**d**, Zero-field magnetic-force image of the magnetic vortex (**b**), where the dark spot at the disc centre reveals the core prepared in the $p = +1$ (**c**) polarity state. The opposite configuration is the $p = -1$ (**d**) polarity state.

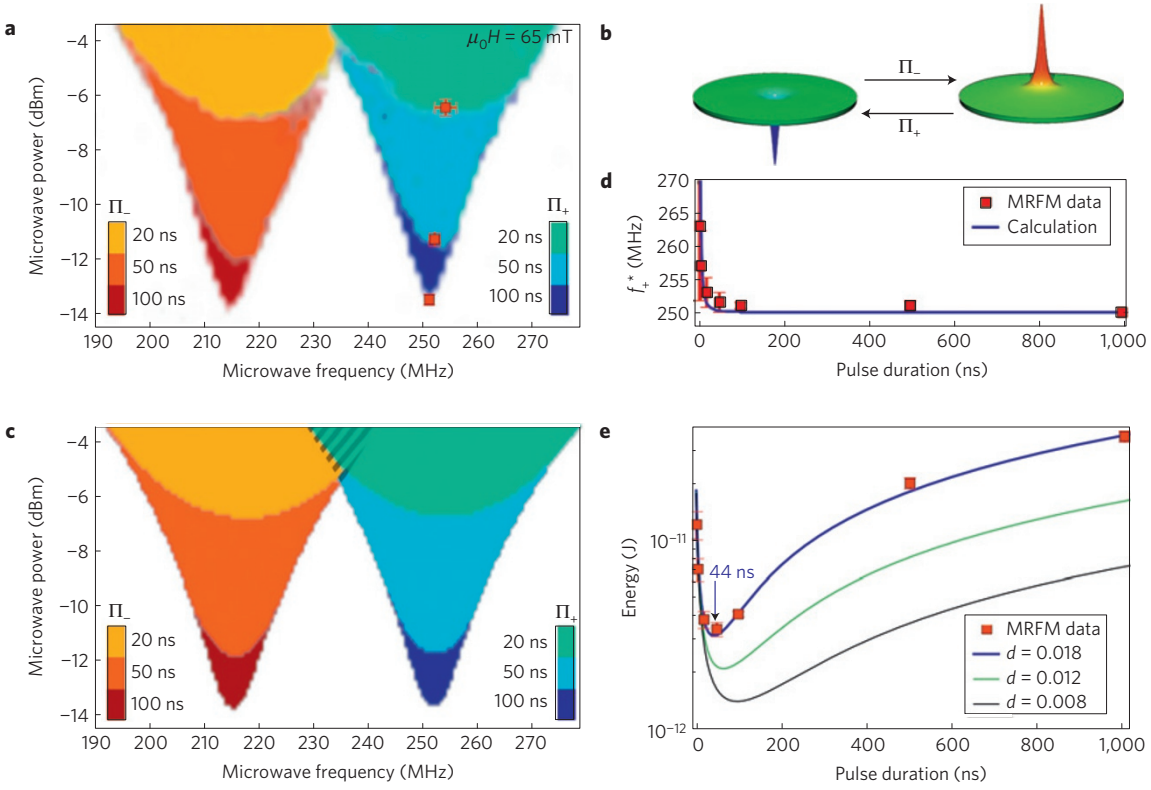

Figure 2 | Vortex-core resonant reversal by a single microwave pulse. a,**b**, Efficiency (**a**) of the Π_- and Π_+ pulses (**b**) to reverse the vortex core at $\mu_0 H = 65$ mT measured as a function of power and frequency (stepped by increments of 0.3 dBm and 1.2 MHz). For each pulse type, a coloured pixel (Π_-, red shade; Π_+, blue shade) marks a successful reversal. The transparency gives the switching probability averaged over 16 attempts. Experiments corresponding to three values of the pulse duration w are shown. For each w we define (f_+^*, P^*), the optimal working point of the Π_+ pulse located at the bottom of the corresponding contour plot (see red squares). **c**, Numerical calculation (see Methods) of the experiments presented in **a**. This calculation is not valid within the shaded area, where multiple vortex-core reversals can occur. **d**,**e**, Experimental (red squares) and calculated (lines) dependencies on w of the optimal frequency f_+^* (**d**) and of the optimal pulse energy $E^* = P^* w$ (**e**). The experimental points are obtained from the analysis of data sets similar to those presented in **a**, where w is varied from 1 μs down to 3 ns (the three red squares close to the minimum energy in **e** are inferred from those shown in **a**). The best agreement is obtained for a damping ratio $d^*_{\text{forced}} = 0.018$, that is, a characteristic decay time $\tau_{\text{forced}} = 35 \pm 4$ ns. The absolute value of the energy is also fitted in the calculation, which enables us to extract the critical velocity for vortex-core reversal, $V_c \simeq 190$ m s^{-1} (see Methods). Error bars on f_+^* and E^* are absolute minima and maxima resulting from experimental uncertainties in **a** on the optimal working point (f_+^*, P^*) associated with each pulse duration.

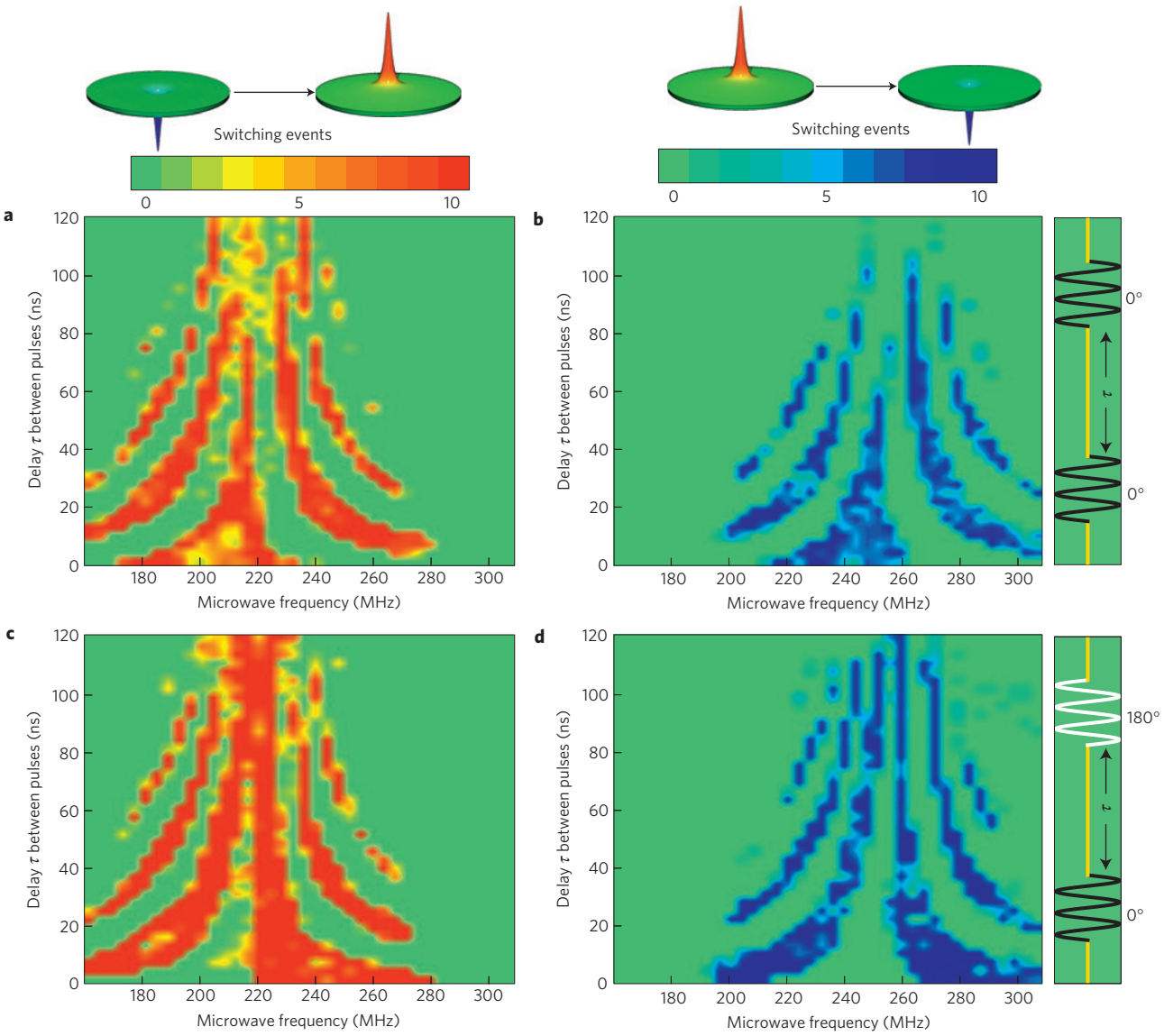

Figure 3 | Oscillatory dependence of the vortex-core reversal efficiency on frequency and delay between two consecutive pulses. a–d, Number of switching events out of ten attempts as a function of the delay τ separating the two pulses ($w = 9$ ns, $P = -1.8$ dBm) and of the carrier microwave frequency (stepped by increments of 3 ns and 4 MHz, respectively). The bias magnetic field is $\mu_0 H = 65$ mT. The initial polarity state is $p = -1$ in the left-hand graphs (**a**,**c**) and $p = +1$ in the right-hand graphs (**b**,**d**). As depicted in the right-hand panels, the phase difference between the two pulses is zero in the upper graphs (**a**,**b**) and π in the lower graphs (**c**,**d**).

w, frequency f and power P is applied, and the final polarity state is read using an MRFM. An opaque coloured pixel marks pulse settings for which reversals are recorded with a 100% success rate, whereas a blank pixel means that no reversal is recorded. The contour plots presented in Fig. 2a with different shades of red (blue) show the superposition of the results for Π_- (Π_+) pulses with three different durations w:100, 50 and 20 ns.

The frequency splitting introduced by the perpendicular bias field clearly appears in Fig. 2a. Due to the resonant character of the investigated switching process, a pronounced minimum in the power level required to reverse the vortex core is observed at a frequency $f_-{}^*$ ($f_+{}^*$) close to the gyrotropic frequency associated with the initial core polarity, for each duration of the Π_- (Π_+) pulses. This frequency discrimination introduced by H enables most of the recorded results to be fully deterministic.

The minimum power P^* required to reverse the core polarity increases as the pulse duration w decreases. We have plotted the dependencies on w of the optimal frequency $f_+{}^*$ (Fig. 2d) and of the optimal pulse energy $E^* = P^* w$ (Fig. 2e). In these plots, w ranges from 1 μs down to 3 ns, with experimental points obtained from the analysis of data sets similar to those presented Fig. 2a. There is a clear minimum in the optimal pulse energy that occurs around $w = 50$ ns. The position of this minimum yields an estimation of the characteristic decay time. If the pulse duration exceeds this characteristic time, the vortex-core dynamics reaches steady state before the end of the pulse; that is, the pulse duration is uselessly too long. In contrast, if the pulse duration is shorter than this characteristic time, some energy is wasted outside the resonance line. Due to the transient response of the vortex core to the excitation pulse, the optimal frequency $f_+{}^*$ measured for pulses shorter than 50 ns shifts to higher frequency[9] (see Fig. 2d), a general behaviour of any harmonic oscillator forced on timescales shorter than its decay time.

To be more quantitative, we have carried out a numerical calculation based on the analytical approach developed for zero applied magnetic field[9], with the new ingredient that, owing to

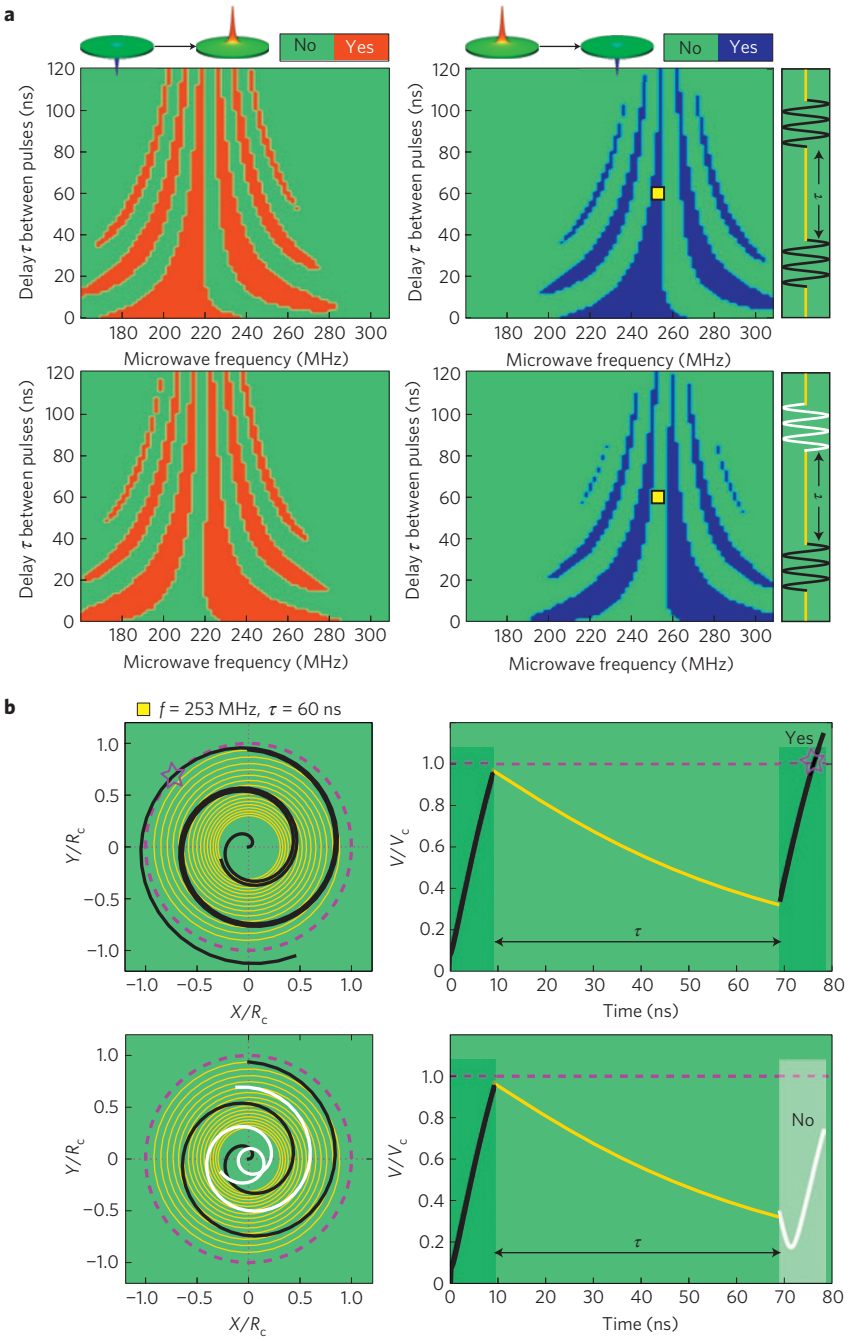

Figure 4 | Phase-coherent control of vortex-core reversal. a, Numerical calculation (see Methods) of the double-pulse sequences presented in Fig. 3. The best agreement is obtained for a characteristic decay time $\tau_{free} = 53 \pm 6$ ns in the free regime. **b**, Associated vortex-core trajectory (left) and velocity (right) versus time plotted for two Π_+ pulses with settings $\tau = 60$ ns and $f = 253$ MHz (see yellow squares in **a**). For these settings, the vortex core is reversed when the phase difference between the pulses is equal to zero (top, see star) and not reversed when it is equal to π (bottom).

the bias perpendicular field, f_- and f_+ are distinct frequencies. The trajectory of the vortex core subjected to the microwave field pulse is calculated using Thiele's equation[27], and Guslienko's criterion[8] for core velocity is used to determine whether the polarity is switched by the end of the pulse. The behaviour of the optimal pulse energy as a function of w can be reproduced with an analytical formula where the damping ratio d^*_{forced} is an adjustable parameter (blue solid line in Fig. 2e). The best fit is obtained for $d^*_{forced} = 0.018$, corresponding to a characteristic decay time $\tau_{forced} = 1/(d^*_{forced} 2\pi f_+) \simeq 35$ ns. The predicted optimal pulse duration is $w_{min} = 1.26\tau_{forced} \simeq 44$ ns (see Methods for details). Fig. 2c illustrates the good agreement of the model with the experimental data of Fig. 2a on the whole range of pulse parameters.

The significant result here is that the damping ratio $d^*_{forced} = 0.018$ inferred in the forced regime close to the core-reversal threshold is more than twice the value measured in the small-oscillation regime of the gyrotropic mode, found to be $d_{vortex} = 0.0075$ (corresponding to a decay time $\tau_{vortex} = 85$ ns). The damping ratio d_{vortex} is itself about three times larger than the Gilbert constant, measured from the linewidth in the perpendicularly saturated state of the NiMnSb disc and found to be $\alpha_{LLG} = 0.0025$ (see Supplementary Fig. S1). The difference between d_{vortex} and α_{LLG} corresponds to the expected increase due to topological

renormalization[27,28]. This enhancement is produced by the strongly inhomogeneous spatial distribution of magnetization in the undistorted vortex state compared with the perpendicularly saturated state. Our experimental results of Fig. 2 give a quantitative estimation of the damping ratio $d^*_{\rm forced}$ for the vortex distorted by large oscillations[8,14]. In a further step, it would be interesting to evaluate how much of the observed increase of $d^*_{\rm forced}$ against $d_{\rm vortex}$ is due to topological renormalization between the distorted and undistorted vortex states. As can be seen in Fig. 2e, a practical consequence of this increase is to decrease the optimal pulse duration $w_{\rm min}$ and to increase the corresponding minimum pulse energy.

Next, we investigate in Fig. 3 the vortex-core dynamics in the free-decay regime by monitoring the core reversal induced by two consecutive microwave pulses. In these experiments, the pulse duration is set to $w = 9$ ns and the power to $P = -1.8$ dBm, that is, slightly below the minimum power $P^* = -1$ dBm required to reverse the core polarity p for such a short pulse. In contrast to a single pulse, two pulses separated by a delay τ (Fig. 3a, $\Pi_- - \tau - \Pi_-$; Fig. 3b, $\Pi_+ - \tau - \Pi_+$) can reverse p. The striking oscillatory dependence on the pulse carrier frequency and on the delay τ observed in Fig. 3a,b elucidates the phase-coherent coupling between the vortex gyrotropic motion and the microwave excitation. During the pulse duration the gyrotropic motion is forced at the pulse frequency, whereas in the free-decay regime the core oscillates towards its equilibrium position at its natural frequency, thereby acquiring a phase shift with respect to the excitation carrier. As a result, the efficiency of the second pulse to drive the vortex core to the reversal threshold, which is estimated out of ten attempts in Fig. 3, depends on the microwave frequency and on the delay between pulses in an oscillatory manner (the oscillation period scales as the inverse frequency detuning).

To illustrate further this effect of coherence, similar experiments with a π phase shift introduced between the two pulses have been carried out. It is clear that the regions where successful reversal are observed in Fig. 3c and d are complementary to those in Fig. 3a and b, respectively. Thus, phase control of the microwave excitation can trigger vortex-core switching.

Using the same approach as before, it is possible to calculate numerically such experimental phase diagrams. An excellent agreement with experiments is achieved, as can be seen in Fig. 4a. In Fig. 4b, we have plotted the calculated vortex-core trajectory and velocity as a function of time corresponding to two consecutive Π_+ pulses at $f = 253$ MHz separated by a 60 ns delay. In the top graphs, there is no phase shift between pulses and the time delay is such that the second pulse is efficient to amplify the gyrotropic motion from the beginning of the pulse, in contrast to the bottom graphs, where a π phase shift is set between pulses. As a result, the vortex core is not reversed by the end of the second pulse in the latter case, whereas it is in the former. The obtained data sets also enable us to fit the free-decay time, and the best agreement with the experiment is obtained for $\tau_{\rm free} \simeq 53$ ns. Analysis of the difference of this value from $\tau_{\rm forced}$ should further shed some light on the precise nonlinear nature of magnetic dissipation close to the reversal threshold and on its dependence on the amplitude of the vortex-core motion.

Methods

Sample preparation. The magnetic nanodisc (thickness 44 nm, diameter 1 μm) was patterned by standard e-beam lithography and ion-milling techniques from an extended film of NiMnSb grown by molecular-beam epitaxy on an InP(001) substrate[29]. A 50-nm-thick Si_3N_4 cap layer was deposited on top of the disc for protection and a broadband coplanar microwave antenna (300-nm-thick Au) was subsequently evaporated on top of the patterned disc. The width of the antenna constriction above the disc is 5 μm (see Supplementary Fig. S2).

Microwave set-up. Injecting a microwave current from a synthesizer inside the antenna produces an in-plane linearly polarized microwave magnetic field h, oriented perpendicular to the stripe direction. To apply two consecutive pulses separated by a variable delay τ, the carrier of the cw excitation is split into two branches, each of them being gated by independent mixers before being recombined. A phase shift can be introduced between the two branches using a delay line. The typical rise and fall times of pulses are 0.8 ns and the control on the delay τ is better than 0.1 ns. The calibration of the amplitude of h yields the value $\mu_0 h = 1.05$ mT with an error bar of 25% for a 0 dBm input power in the antenna. Therefore, the microwave power range in Fig. 2a corresponds to microwave field amplitude ranging from 0.2 to 0.7 mT, the power in double-pulse experiments of Fig. 3a to $\mu_0 h = 0.85$ mT and the power employed to read the polarity to $\mu_0 h = 0.1$ mT.

Initialization pulse. A Π_+ pulse with settings $w = 50$ ns, $f = f_+$, $P = -11$ dBm (ref. 15) is used to set the initial polarity state to $p = -1$. In fact, such an initialization pulse does not affect the $p = -1$ state and it transforms $p = +1$ into $p = -1$ (see Fig. 2a). Similarly, a Π_- pulse ($w = 50$ ns, $f = f_-$, $P = -11$ dBm) is used to set the initial polarity state to $p = +1$.

MRFM detection. The MRFM set-up[23] is located inside a vacuum chamber (10^{-6} mbar) and operates at room temperature. The cantilever is an Olympus Biolever (spring constant $k \simeq 5$ mN m^{-1}) with a 800-nm-diameter sphere of soft amorphous Fe (with 3% Si) glued to its apex. MRFM spectroscopy is achieved by placing the centre of the magnetic spherical probe above the centre of the NiMnSb nanodisc. The separation between the sample and the probe is $s = 1.5$ μm. The probe senses the dipolar force F_z proportional to the perpendicular component M_z of the magnetization of the nanodisc (see Fig. 1a). Ferromagnetic resonance spectra are obtained as a function of the microwave excitation frequency at a fixed bias field H. The microwave modulation is a cyclic absorption sequence, where the microwave power is switched on and off at the cantilever resonance frequency, $f_c \simeq 11.8$ kHz. The MRFM signal originates from the cyclic diminution of M_z of the nanodisc synchronous with the absorption of the microwave field[16,23]. The resulting force modulated at the mechanical resonance of the cantilever force produces a cantilever vibration amplitude enhanced by its quality factor $Q \simeq 4{,}000$, which is optically detected.

Numerical calculations. The calculations presented in Figs 2 and 4 are based on the linearized Thiele equation[27], an effective equation of motion for the vortex-core position $\boldsymbol{X}$ in the disc plane:

$$-\boldsymbol{G}\times\dot{\boldsymbol{X}} - \hat{D}\dot{\boldsymbol{X}} + \kappa\boldsymbol{X} + \mu[\hat{\boldsymbol{z}}\times\boldsymbol{h}] = 0 \qquad (1)$$

The first term is the gyroforce ($\boldsymbol{G}$ is the gyrovector), the second one is the damping ($d = -D/|G|$), the third one is the restoring force (κ is the stiffness coefficient) and the last one is the Zeeman energy with the spatially uniform external field $\boldsymbol{h}$ ($\hat{\boldsymbol{z}}$ is the unit vector normal to the disc plane and details of μ and previously mentioned coefficients can be found in refs 3,28). The resonant frequency of vortex-core gyration is $\omega_G = \kappa/|G|$. From equation (1) we can find the instantaneous position $\boldsymbol{X}(t)$ and the velocity $v(t)$ of the vortex core in the presence or absence of the harmonic excitation field $h(t)$, as derived in the supplementary documents of ref. 9. If Guslienko's criterion on critical velocity[8] is met at some time of the simulated pulse sequence ($v(t) > V_c$), the vortex core is assumed to have switched. Experimental sample size, gyrotropic frequencies f_- and f_+ associated with each polarity, and nonlinear redshift of the frequency (3%) are used in our calculation. The minimal excitation amplitude $h_c(\omega, w)$ to reach V_c by the end of the pulse depends[9] on the excitation frequency ω and on the pulse duration w. Minimization of the energy $E \propto w{h_c}^2(\omega, w)$ with respect to ω yields the dependence on w of the optimal frequency ${f_+}^*$ plotted in Fig. 2d and of the optimal pulse energy E^* plotted in Fig. 2e:

$$E^*(w) = w\frac{{h_c}^2(w)}{a} = \left(\frac{6dV_c}{a\gamma R}\right)^2 \frac{w}{1 + e^{-2d\omega_G w} - 2e^{-d\omega_G w}} \qquad (2)$$

In this expression, a is an experimental conversion factor between the input power in the antenna and h^2 determined from calibration; R is the radius of the nanodisc. Therefore, two independent parameters are used to adjust the calculation with the data in Fig. 2e: the damping ratio d to fit the overall shape (position of the minimum) and the critical velocity V_c to fit the absolute value of the energy. The optimal pulse duration $w_{\rm min}$ corresponding to the minimum energy ${E_{\rm min}}^*$ follows from equation (2): $w_{\rm min} = 1.26/(d^*_{\rm forced}\omega_G) = 1.26\tau_{\rm forced}$ (for the blue solid line in Fig. 2e, $d^*_{\rm forced} = 0.018$, $\tau_{\rm forced} = 35$ ns, hence ${E_{\rm min}}^*$ is reached for $w_{\rm min} = 44$ ns). The fitted critical velocity in our NiMnSb disc is $V_c \simeq 190$ m s^{-1}, in good agreement with the expected value[9] of 225 m s^{-1} (the exchange constant of NiMnSb is $A_{ex} = 6$ pJ m^{-1}; ref. 30). The same parameters are used in the calculations of Figs 2 and 4. In Fig. 4, the only new fitting parameter is the characteristic time $\tau_{\rm free}$ of the vortex-core free decay (the relaxation is assumed to be exponential). We also allow a fine adjustment of the phase shift between the two pulses to obtain the best agreement with the data (25° in the 'zero-phase-shift' experiment and 190° in the 'π-phase-shift' experiment; these small differences are ascribed to an imperfect delay line in the experimental pulse set-up).

Received 5 May 2010; accepted 7 September 2010; published online 31 October 2010

References

1. Miramond, C., Fermon, C., Rousseaux, F., Decanini, D. & Carcenac, F. Permalloy cylindrical submicron size dot arrays. *J. Magn. Magn. Mater.* **165,** 500–503 (1997).
2. Cowburn, R. P., Koltsov, D. K., Adeyeye, A. O., Welland, M. E. & Tricker, D. M. Single-domain circular nanomagnets. *Phys. Rev. Lett.* **83,** 1042–1045 (1999).
3. Guslienko, K. Y. Magnetic vortex state stability, reversal and dynamics in restricted geometries. *J. Nanosci. Nanotechnol.* **8,** 2745–2760 (2008).
4. Shinjo, T., Okuno, T., Hassdorf, R., Shigeto, K. & Ono, T. Magnetic vortex core observation in circular dots of permalloy. *Science* **289,** 930–932 (2000).
5. Wachowiak, A. *et al.* Direct observation of internal spin structure of magnetic vortex cores. *Science* **298,** 577–580 (2002).
6. Hertel, R. & Schneider, C. M. Exchange explosions: Magnetization dynamics during vortex–antivortex annihilation. *Phys. Rev. Lett.* **97,** 177202 (2006).
7. Hertel, R., Gliga, S., Fähnle, M. & Schneider, C. M. Ultrafast nanomagnetic toggle switching of vortex cores. *Phys. Rev. Lett.* **98,** 117201 (2007).
8. Guslienko, K. Y., Lee, K-S. & Kim, S-K. Dynamic origin of vortex core switching in soft magnetic nanodots. *Phys. Rev. Lett.* **100,** 027203 (2008).
9. Lee, K-S. *et al.* Universal criterion and phase diagram for switching a magnetic vortex core in soft magnetic nanodots. *Phys. Rev. Lett.* **101,** 267206 (2008).
10. Waeyenberge, B. V. *et al.* Magnetic vortex core reversal by excitation with short bursts of an alternating field. *Nature* **444,** 461–464 (2006).
11. Yamada, K. *et al.* Electrical switching of the vortex core in a magnetic disk. *Nature Mater.* **6,** 270–273 (2007).
12. Curcic, M. *et al.* Polarization selective magnetic vortex dynamics and core reversal in rotating magnetic fields. *Phys. Rev. Lett.* **101,** 197204 (2008).
13. Weigand, M. *et al.* Vortex core switching by coherent excitation with single in-plane magnetic field pulses. *Phys. Rev. Lett.* **102,** 077201 (2009).
14. Vansteenkiste, A. *et al.* X-ray imaging of the dynamic magnetic vortex core deformation. *Nature Phys.* **5,** 332–334 (2009).
15. Pigeau, B. *et al.* A frequency-controlled magnetic vortex memory. *Appl. Phys. Lett.* **96,** 132506 (2010).
16. de Loubens, G. *et al.* Bistability of vortex core dynamics in a single perpendicularly magnetized nanodisk. *Phys. Rev. Lett.* **102,** 177602 (2009).
17. Park, J. P., Eames, P., Engebretson, D. M., Berezovsky, J. & Crowell, P. Imaging of spin dynamics in closure domain and vortex structure. *Phys. Rev. B* **67,** 020403(R) (2003).
18. Novosad, V. *et al.* Magnetic vortex resonance in patterned ferromagnetic dots. *Phys. Rev. B* **72,** 024455 (2005).
19. Keavney, D. J., Cheng, X. M. & Buchanan, K. S. Polarity reversal of a magnetic vortex core by a unipolar, nonresonant in-plane pulsed magnetic field. *Appl. Phys. Lett.* **94,** 172506 (2009).
20. Thomas, L. *et al.* Oscillatory dependence of current-driven magnetic domain wall motion on current pulse length. *Nature* **443,** 197–200 (2006).
21. Thirion, C., Wernsdorfer, W. & Mailly, D. Switching of magnetization by nonlinear resonance studied in single nanoparticles. *Nature Mater.* **2,** 524–527 (2003).
22. Ivanov, B. A. & Wysin, G. M. Magnon modes for a circular two-dimensional easy-plane ferromagnet in the cone state. *Phys. Rev. B* **65,** 134434 (2002).
23. Klein, O. *et al.* Ferromagnetic resonance force spectroscopy of individual submicron-size samples. *Phys. Rev. B* **78,** 144410 (2008).
24. de Loubens, G. *et al.* Magnetic resonance studies of the fundamental spin-wave modes in individual submicron Cu/NiFe/Cu perpendicularly magnetized disks. *Phys. Rev. Lett.* **98,** 127601 (2007).
25. Heinrich, B. *et al.* Magnetic properties of NiMnSb(001) films grown on InGaAs/InP (001). *J. Appl. Phys.* **95,** 7462–7464 (2004).
26. Thiaville, A., García, J. M., Dittrich, R., Miltat, J. & Schrefl, T. Micromagnetic study of Bloch-point-mediated vortex core reversal. *Phys. Rev. B* **67,** 094410 (2003).
27. Thiele, A. A. Steady-state motion of magnetic domains. *Phys. Rev. Lett.* **30,** 230–233 (1973).
28. Guslienko, K. Y. Low-frequency vortex dynamic susceptibility and relaxation in mesoscopic ferromagnetic dots. *Appl. Phys. Lett.* **89,** 022510 (2006).
29. Bach, P. *et al.* Molecular-beam epitaxy of the half-Heusler alloy NiMnSb on (In,Ga)As/InP(001). *Appl. Phys. Lett.* **83,** 521–523 (2003).
30. Ritchie, L. *et al.* Magnetic, structural, and transport properties of the Heusler alloys Co_2MnSi and NiMnSb. *Phys. Rev. B* **68,** 104430 (2003).

Acknowledgements

This research was partially supported by the French Grant Voice ANR-09-NANO-006-01, EU Grants DynaMax FP6-IST-033749 and Master NMP-FP7-212257. The authors acknowledge discussions with V. S. Tiberkevich, A. N. Slavin and K. Y. Guslienko.

Author contributions

B.P., G.d.L. and O.K. conceived and carried out the MRFM and microwave experiments and carried out the simulations. A.R., F.L., G.S. and L.W.M. optimized and realized the epitaxial growth of NiMnSb and the subsequent nanofabrication process. G.d.L., B.P. and O.K. co-wrote the paper. All authors discussed the results and commented on the manuscript.

Additional information

The authors declare no competing financial interests. Supplementary information accompanies this paper on www.nature.com/naturephysics. Reprints and permissions information is available online at http://npg.nature.com/reprintsandpermissions. Correspondence and requests for materials should be addressed to G.dL.